International Journal Of
Industrial Electronics Control and Optimization
Print ISSN: 3517-2645
Online ISSN: 3568-2645
Homepage: https://ieco.usb.ac.ir/

Radiation Improvement of Low-Profile Microstrip Antenna by Utilizing AMC Surface for MIMO and Wireless Systems

Hossein Malekpoor[1] | Mehdi Hamidkhani[2]

Department of Electrical Engineering, Faculty of Engineering, Arak University, Arak, 38156-8-8349, Iran[1]
Department of Electrical Engineering, Isfahan (khorasgan) Branch, Islamic Azad University, Isfahan, Iran[2]
Corresponding author's email: h-malekpoor@araku.ac.ir

Article Info

Article type:
Research Article

Article history:
Received: 06-May-2024
Received in revised form: 17-August-2024
Accepted: 04-October-2024
Published online: 22-June-2025

Keywords:
Artificial Magnetic Conductor,
Printed Antenna,
Multi-Input Multi-Output,
Wideband,
Wireless.

ABSTRACT

A compact microstrip antenna by applying a parasitic artificial magnetic conductor (AMC), is proposed for facilitating 4G and 5G wireless communications. The antenna design includes microstrip dipoles fed by a T-shaped feedline. Notably, the antenna achieves a measured bandwidth of 5.32-6.73 GHz (with $S_{11} \leq$ -10 dB). To enhance performance, a proposed parasitic AMC reflector is integrated into the antenna structure. Incorporating an 8×8 AMC array, the antenna extends its -10 dB measured bandwidth from 4.51 to 6.83 GHz, catering to both 4G and 5G communication standards. Comparative analysis with an antenna lacking AMC reveals a reduced size of 35%, alongside a notable gain of 8 dBi and uni-directional radiation patterns. The efficiency and gain of all elements are approximately 90% and 8 dBi, respectively. Moreover, the introduction of an AMC unit cell, well-founded on a parasitic patch, resonates at 6.15 GHz with a bandwidth extending from 5.21 to 7.10 GHz. Furthermore, the offered equivalent transmission line model of the antenna with the AMC is demonstrated, yielding desirable results. This model accurately predicts the input impedance of the antenna with AMC across a broad frequency band ranging from 4.64 to 6.74 GHz. This comprehensive study demonstrates the effectiveness and versatility of the offered model in characterizing the operating band's behavior of the antenna across a wide frequency band to facilitate its design and optimization for various applications.

I. Introduction

structures have found application across various wireless networks and high-frequency devices [1-4]. Artificial Magnetic Conductor (AMC) structures, which utilize periodic boundary conditions across their operating band, have been increasingly adopted for applications such as cost-effective patch antennas, low-profile antennas, and mode suppression. These structures are particularly valued for their ability to mimic a perfect magnetic conductor over a specific frequency range, leading to enhanced antenna performance. AMCs are advantageous in reducing antenna size and improving radiation efficiency while maintaining a low profile, making them ideal for integration into modern wireless communication systems. By suppressing unwanted modes and enhancing the desired ones, AMCs contribute to the overall efficiency and effectiveness of antenna designs, especially in compact and complex wireless systems. [5-10]. In a recent work [9], a broadband patch array featuring EBG-AMCs was introduced to enhance the wireless transmission rate for 5G communication. The investigation of periodic AMC surfaces without vias has been explored in [11-18]. In [16], an EBG mushroom reflector with a two-layer configuration was utilized, resulting in a 60% size reduction. However, achieving a broad AMC bandwidth remains a significant challenge [19], prompting numerous efforts [20-22]. In [22], an AMC unit cell at a resonance of 6.2 GHz with a bandwidth of 4.4% was reported, exhibiting acceptable angular stability.

The Multi-Input Multi-Output (MIMO) method has become a pivotal technology in recent wireless communication systems, primarily due to its capability to transmit high data rates while minimizing latency [23-24]. This method leverages multiple antennas at both the transmitter and receiver ends to enhance communication reliability and increase channel capacity. A critical aspect of MIMO system design is achieving high port isolation, which

Copyright © *H. Malekpoor, et al.*
Publisher: University of Sistan and Baluchestan

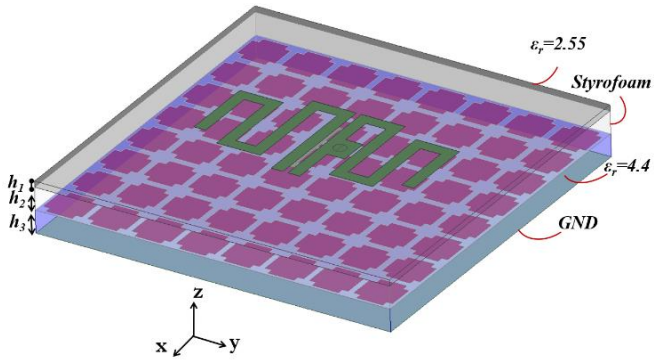
helps reduce interference between antenna elements and improves overall system performance. Various techniques have been explored to achieve this, including the use of orthogonal modes, mirrored elements, and different propagation modes [25-28]. These approaches are aimed at enhancing the isolation between the antenna ports, thereby ensuring better performance of MIMO antennas in terms of signal clarity and transmission efficiency.

Numerous techniques have been proposed to integrate broad AMC surfaces with microstrip antennas [29-30]. For instance, a low-profile circular polarized microstrip antenna incorporating AMC was presented in [30] to boost gain and bandwidth. Additionally, the development of two-layer boards has been prevalent in achieving improved radiation properties in most literature. The electromagnetic properties and applications of AMCs have led to a diverse range of studies aimed at enhancing antenna performance and miniaturization [31-38]. A low-profile and wide-axial-ratio-beamwidth (ARBW) circularly polarized antenna loaded with a honeycomb-shaped artificial magnetic conductor (AMC) is presented [36].

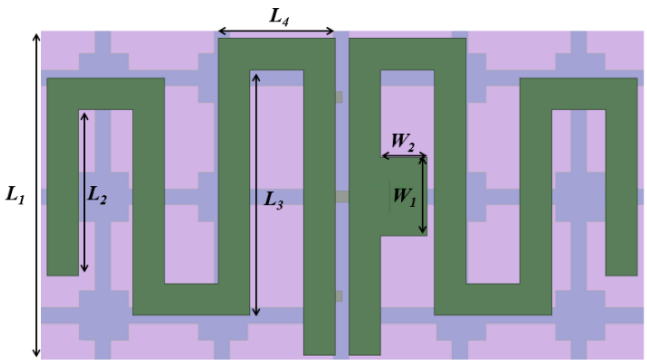
This study specifically concentrates on a proposed antenna utilizing AMC for MIMO applications. Initially, a low-profile wideband microstrip antenna configured with two printed dipoles fed by a T-shaped feedline is designed to enlarge the impedance bandwidth. Subsequently, a parasitic AMC is demonstrated to intensify at 6.15 GHz (5.21-7.10 GHz). The printed antenna with an 8×8 parasitic AMC reflector exhibits a measured -10 dB bandwidth of 4.55-6.83 GHz, suitable for 5G and MIMO applications. Furthermore, the proposed equivalent transmission line model is designed to offer a simplified yet accurate representation of the antenna integrated with the AMC structure. This model enables efficient analysis and optimization of the antenna's input impedance, which is crucial for achieving the desired performance characteristics.

II. Printed Microstrip Antenna with Planar AMC

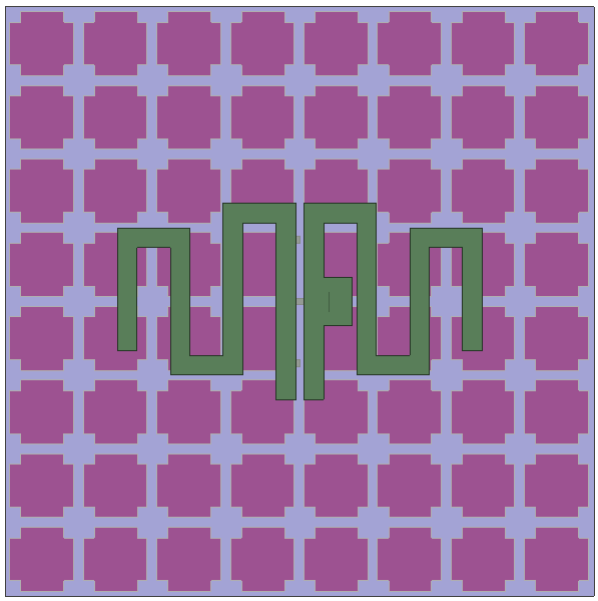
Figure 1 illustrates the overall schematic of the printed antenna, which consists of two elements featuring folded dipoles mounted on Taconic TLT substrate (98.4 mm×98.4 mm, with a thickness of h_1=0.8 mm, dielectric constant ε_r=2.55, and a loss tangent of 0.0006). Positioned beneath the antenna is a periodic parasitic AMC surface, separated by an air gap (Styrofoam layer) from the antenna to facilitate broadband operation. The optimal air gap distance, denoted



(a)



(b)



(c)

Fig.1. Structure of the suggested antenna by AMC reflector (a) 3D view (b) printed antenna design (c) Top view.

TABLE 1 SIZES OF SUGGESTED STRUCTURE

Parameters	Values (mm)
L_1	16
L_2	8.8
L_3	12
L_4	4.9
W_1	3.2
W_2	2.6
h_1	0.8
h_2	3
h_3	3
m	3
n	6
k	8.1

Figure 2 draws the schematic of a proposed unit cell for the AMC. This unit cell is constructed using an FR4 substrate with a relative permittivity (ε_r) of 4.4 and a thickness (h) of 3 mm. It is optimized with a ground plane measuring 8.1 mm×8.1 mm. The mushroom-type electromagnetic band gap (EBG) surface is modeled using an LC resonator, the calculation of which can be expressed as outlined in [11]:

$$C = \frac{W_{ebg}\varepsilon_0(1+\varepsilon_r)}{\pi}\cosh^{-1}\left(\frac{2W_{ebg}+g}{g}\right) \quad (1)$$

$$L = \mu_0 h \quad (2)$$

$$BW = \frac{1}{\eta}\sqrt{\frac{L}{C}} \quad (3)$$

The proposed equivalent transmission line model for the printed array with the AMC structure is designed to capture the detailed electrical characteristics and behavior of the antenna system. This model simplifies the complex interactions within the antenna into a combination of lumped elements and transmission line segments, making it easier to analyze and optimize the system's performance. Below is an outline of the key components in the proposed model [20]:

$$C_1 = \frac{\varepsilon_e\varepsilon_0 L_e W}{2h}\cos^{-2}\left(\frac{\pi y_0}{L}\right) \quad (4)$$

$$L_1 = \frac{1}{(2\pi f_r)^2 C_1} \quad (5)$$

$$R_1 = \frac{Q}{\omega C_1} \quad (6)$$

$$Q = \frac{c\sqrt{\varepsilon_e}}{4 f_r h} \quad (7)$$

$$C_c = \frac{-(C_1+C_2)+\sqrt{((C_1+C_2)^2 - 4C_1C_2(1-1/C_p{}^2))}}{2} \quad (8)$$

$$C_p = \frac{1}{\sqrt{Q_1 Q_2}} \quad (9)$$

$$C_2 = C_1\Delta C/(C_1+\Delta C) \quad (10)$$

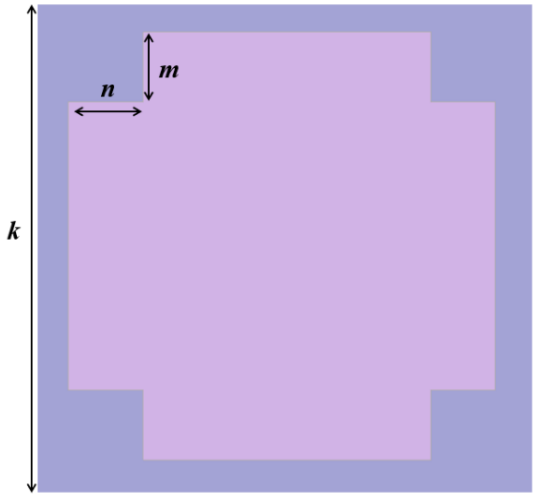


Fig. 2. AMC design.

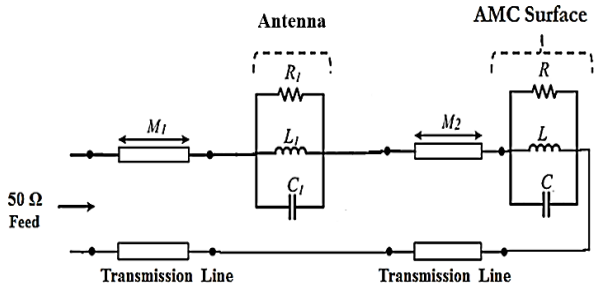


Fig. 3. Introduced equivalent transmission line model

The proposed model in Fig. 3 incorporates various parameters to accurately represent the behavior of the microstrip antenna with the AMC. Here are the key components and their significance. This model for the proposed printed antenna (PDA) involves two RLC resonators because of the symmetric patches. The two symmetric folded strips are represented as L_1C_1 and L_2C_2 elements according to Fig. 3. Additionally, the air ap height between the antenna and the AMC is modeled by the transmission line M_2. Furthermore, an LC resonator is regarded for the periodic surface.

The parameters obtained in equations (4)-(10) are applied to the conventional patch, and the element values of the model are determined using the Agilent Advanced Design System (ADS) simulator, utilizing the method of moments (MOM). The optimized values of the lumped elements which are applied in the model are as follows: R_1=50 Ω, C_1=2.64 pF, L_1=0.241 nH, R=72 Ω, C=0.57 pF, L=0.04 nH, and M_1=3.13 mm.

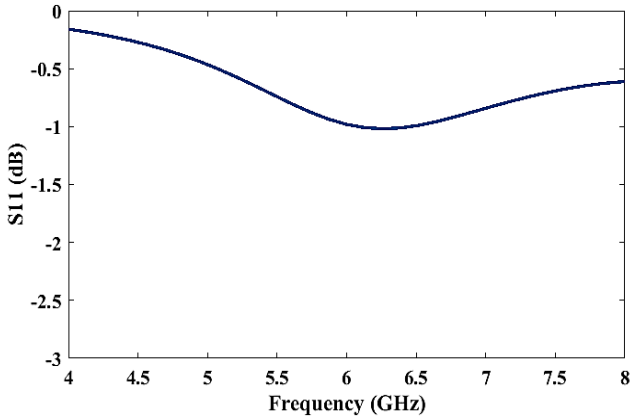
III. Experimental and Simulation Results

Figure 4 shows the reflection magnitude and phase characteristics of the proposed artificial magnetic conductor (AMC) at an incident angle (θ) of 0˚. The simulated results exhibit a ±90˚ reflection phase within the frequency range of 5.21-7.10 GHz, with a resonance occurring at 6.15 GHz. Compared to previous research [11, 20-22], the suggested AMC demonstrates significantly improved characteristics. The design features a symmetric unit cell, ensuring identical responses for both Transverse Electric (TE) and Transverse Magnetic (TM) waves, which enhances the consistency and reliability of the AMC's performance. Moreover, the proposed AMC offers a notably broader bandwidth of approximately 2 GHz, which is a substantial improvement over earlier designs. This broader bandwidth is achieved while maintaining acceptable stability across the AMC's operational range, making it particularly well-suited for broadband applications within the C-band.

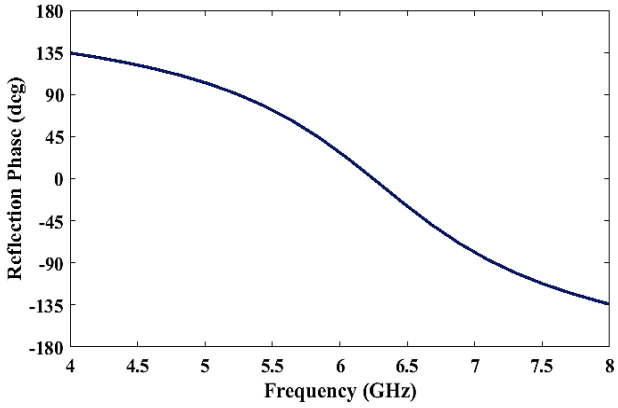
Figure 5 illustrates the S-parameters of the antenna design with and without the AMC. The antenna lacking AMC exhibits a measurement band from 5.32 to 6.73 GHz (22.4%) for S_{11}< -10 dB. Conversely, the antenna equipped with the AMC demonstrates a -10 dB measured bandwidth spanning from 4.51 to 6.83 GHz, representing a bandwidth improvement of more than double.

The dimensions of the antenna without the AMC are as follows: width×length×height; 0.436λL, 0.436λL, and 0.014λL, respectively. In comparison, the dimensions of the antenna with the AMC are 0.362λL, 0.362λL, and 0.101λL, respectively, leading to a size reduction of 35%. Figure 5 (b) illustrates the results of the proposed equivalent model, implemented using ADS software. The simulation results cover 4.64-6.74 GHz, showcasing a well agreement with the measured results. This indicates that the equivalent model accurately captures the electrical behavior of the printed array with the AMC, providing valuable insights for the design and optimization of the antenna system. Simulated S-parameters of the antenna with AMC for various lengths of the parameters m and n are depicted in Figure 6. Figure 7 illustrates the variations in the height of the air gap, h_2, between the antenna and the AMC.

The maximum gain of the proposed antenna with the parasitic AMC across the bandwidth reaches 8 dBi, as observed in Figure 8.

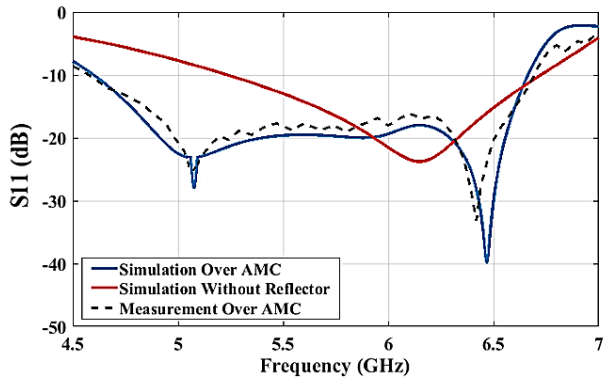


(a)

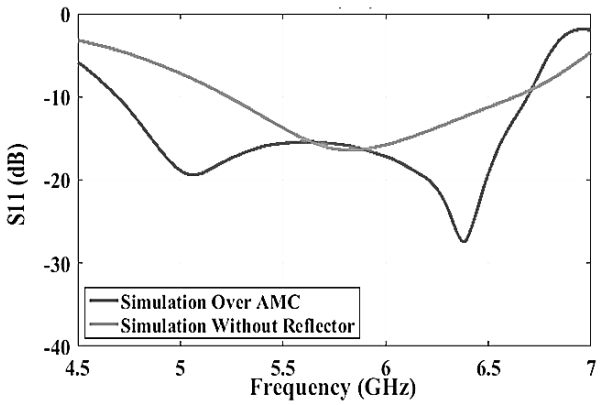


(b)

Fig. 4. Reflection magnitude and phase of AMC for normal incident waves.



(a)



(b)

Fig. 5. Obtained results of S-parameters (a) HFSS (b) proposed model.

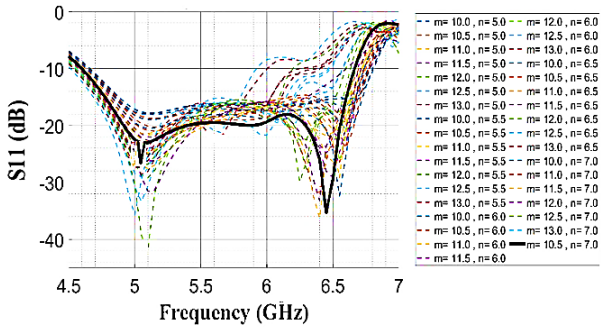


Fig. 6. S-parameters for different lengths of the m and n parameters.

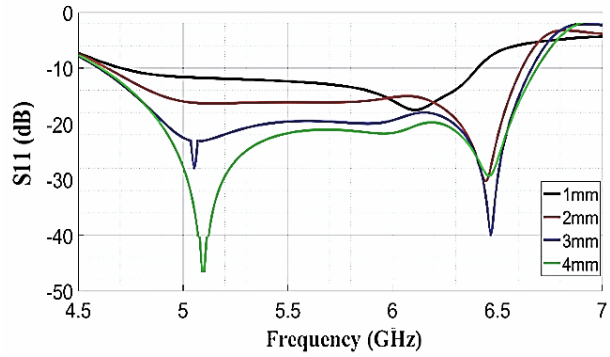


Fig. 7. Simulated S-parameters for different h_2.

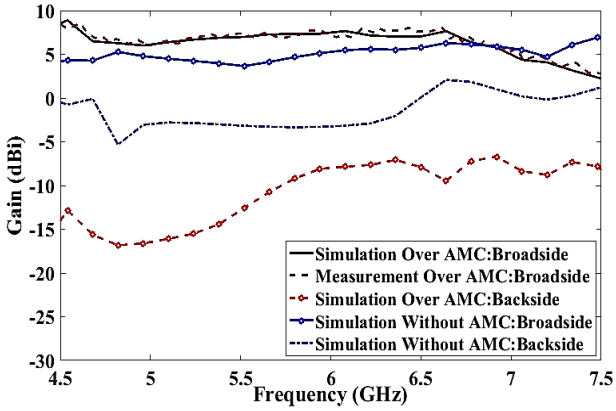
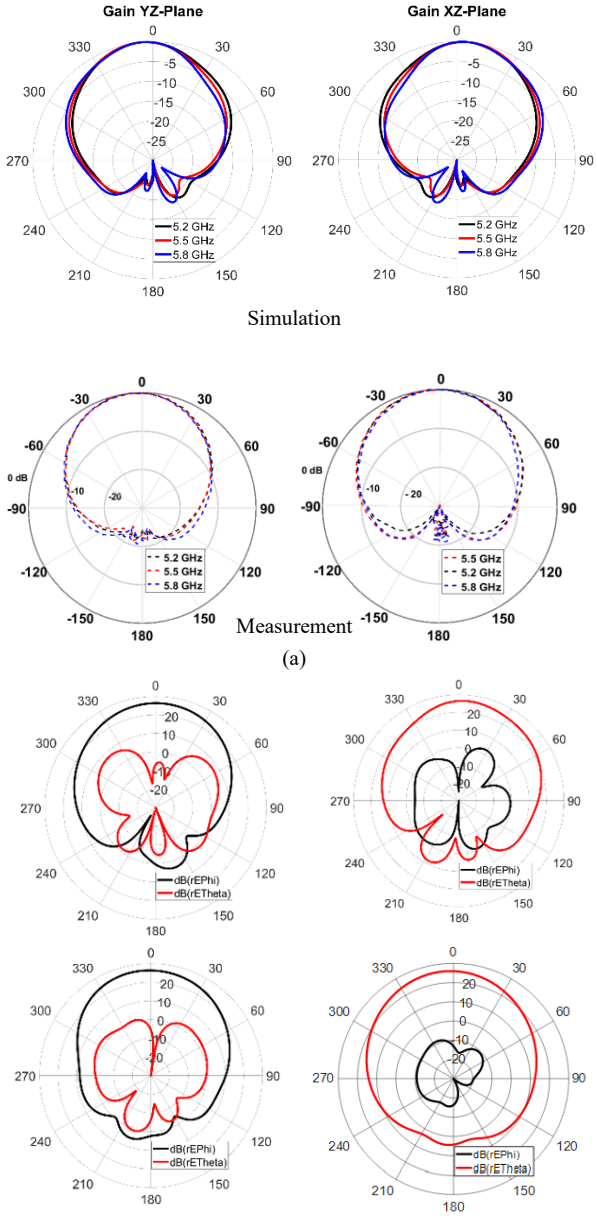
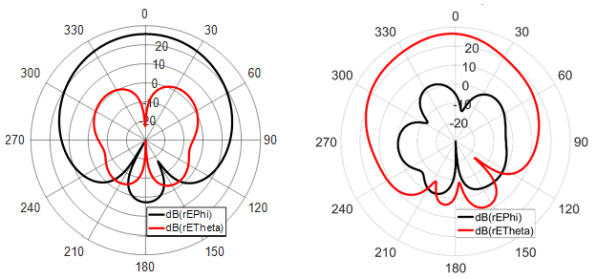


Fig. 8. Gains of the design.



(a)



(b)

Fig. 9. Radiation patterns for (a) gain in XZ and YZ-planes (b) co and cross-pol in XZ and YZ-planes at 5.2, 5.5 and 5.8 GHz.

TABLE 2 COMPARISON STUDY

Proposed design	Measrured bandwidth	Width×Length×Height	Measrured Gain and Efficiency
My work	4.51-6.83 GHz (45.1%)	24.6×24.6×6.8 mm^3 0.362λ_L×0.362 λ_L×0.10λ_L	8 dBi 94%
V-shaped patches coupled by a bowtie dipole with 5×5 AMC array [19]	3–4.1 GHz (31%)	75×75×12.7 mm^3 0.75λ_L×0.75λ_L ×0.127λ_L	7.1 dBi 88%
Patch antenna by using triple-band AMC [20]	3.3–3.42 GHz (3.6%) 5.88-6.1 GHz (3.7%)	64×64×1.6 mm^3 0.71λ_L×0.71λ_L ×0.017λ_L	6.29 dBi 86%
Decoupling techniques using two-port feed network MIMO antenna [24]	3.33-3.67 GHz (9.7%)	70×140×0.8 mm^3 0.77λ_L×1.55λ_L ×0.009λ_L	6 dBi 78%
Printed slot antenna with wideband 3×5 AMC array [29]	2.37-2.50 GHz (5.34%)	100×125×7.5 mm^3 1.02λ_L×0.82λ_L ×0.63λ_L	10.3 dBi 88%
Bow-tie printed antenna with 6×9 fractal AMC array [33]	1.64-1.94 GHz (16.8%)	50×70×25 mm^3 0.27λ_L×0.38λ_L ×0.137λ_L	6.5 dBi 85%
Near-Zero-Index Metamaterial Lens Combined with AMC [34]	6.9–7.9 GHz (13.5%)	76×76×7 mm^3 1.75λ_L×1.75λ_L ×0.160λ_L	13 dBi 90%
M-shaped antenna based on 3×3 Jerusalem Cross AMC array [35]	2.2-2.72 GHz (18%)	67.5×67.5×4.5 mm^3 0.5λ_L×0.5λ_L×0.032λ_L	5 dBi 90%

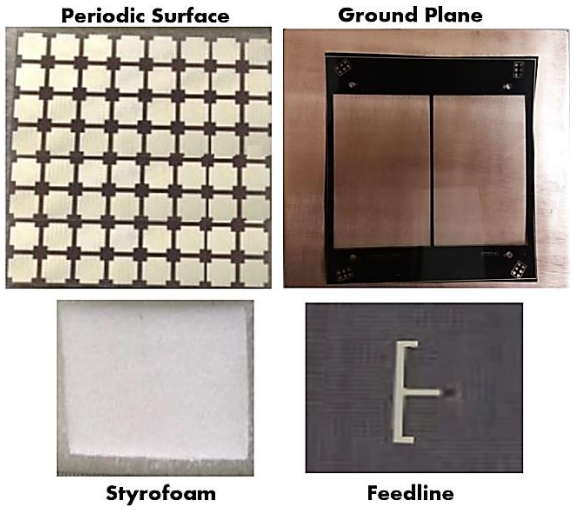


Fig. 10. Images of fabricated cases.

Figure 9 displays the radiation patterns in the XZ-plane and YZ-plane for the antenna design. Table 2 lists the performance of the design with respect to its prominent properties. The proposed design is compared with related works regarding key measurement parameters such as impedance bandwidth, gain, and efficiency. The results demonstrate that the design exhibits superior performance, making it highly suitable for wireless applications Additionally, Figure 10 presents photos of the manufactured antenna.

The proposed antenna is fed using a 50-Ohm probe. For the evaluation of its far-field radiation performance, a measurement setup is employed within an anechoic chamber. In this setup, a well-calibrated standard gain horn antenna acts as the transmitting (TX) antenna, while the prototype antenna serves as the receiving (RX) antenna. The horn antenna is positioned at a far-field distance from the prototype, determined by the formula $2D^2/\lambda$, where D represents the total dimension of the antenna and λ is the wavelength. Amplifiers are utilized to ensure consistent power reception. During the testing process, the prototype antenna is rotated to capture radiation intensity across various orientations. The S-parameters are accurately measured using an Agilent network analyzer.

IV. Conclusions

The introduced AMC design by exhibiting broadband properties within the C-band results in a parasitic patch to cover the range of 5.21-7.10 GHz. The proposed antenna with folded strips using by the AMC structure presents a miniaturized broadband solution for wireless systems. By integrating the 8×8 AMC surface into the antenna, an impressive -10 dB measured bandwidth of 4.51-6.83 GHz (45.1%) is achieved, accompanied by uni-directional radiation patterns and higher gains of up to 8 dBi. Measurement results confirm acceptable efficiency, leading to the conclusion that the design is suitable for wideband

wireless systems. Overall, the proposed equivalent transmission line model aims to provide a simplified yet accurate representation of the antenna with the AMC, allowing for efficient analysis and design optimization of the antenna system.

REFERENCES

[1] H. Malekpoor and S. Jam, "Design, analysis, and modeling of miniaturized multi-band patch arrays using mushroom-type electromagnetic band gap structures," International Journal of RF and Microwave Computer-Aided Engineering., vol. 28, no. 6, pp. 1–13, 2018.

[2] F. Kazemi, "A Compact Antenna with Dual Polarization for Mobile and Wireless Communication," International Journal of Industrial Electronics, Control and Optimization, vol. 6, pp. 73-82, 2023.

[3] S. Jam and H. Malekpoor, "Compact 1×4 patch antenna array by means of EBG structures with enhanced bandwidth", Microw. Opt. Technol. Lett, vol. 58, no. 12, pp. 2983-2989, 2016.

[4] A. A. Althuwayb, "Enhanced radiation gain and efficiency of a metamaterial inspired wideband microstrip antenna using substrate integrated waveguide technology for sub-6 GHz wireless communication systems", Microw Opt Technol Lett, Vol. 63, no. 7, pp 1892-1898, July 2021.

[5] A. Foroozesh, and L. Shafai, "Effects of artificial magnetic conductors in the design of low-profile high-gain planar antennas with high-permittivity dielectric superstrate," IEEE Antennas Wireless Propag. Lett., vol. 8, pp. 10-13, 2009.

[6] Z. F. Dai, Y. Pan, J. J. Huang, L. H. Ye, J. F. Li, H. Jiang, "Low-Profile Broadband Dual-Polarized Dipole Antenna with AMC Reflector," IEEE Antennas Wireless Propag. Lett., vol. 12, pp. 1–5, 2024.

[7] C. Bajaj, D. K. Upadhyay, S. Kumar, B. K. Kanaujia, "GPS-Integrated RFID Antenna With AMC Backing for IoT-Based Sensing and Tracking Applications," IEEE Trans. Antennas Propag., vol. 72, no. 2, pp. 1929 - 1934, 2024.

[8] J. M. Bell, M. F. Iskander, and J. J. Lee, "Ultrawideband hybrid EBG/ferrite ground plane for low-profile array antennas," IEEE Trans. Antennas Propag., vol. 55, no. 1, pp. 4–12, 2007.

[9] D. Nashaat, H. A. Elsadek, E. A. Abdallah, M. F. Iskander, and H. M. E. Hennawy, "Ultrawide bandwidth 2×2 microstrip patch array antenna using electromagnetic band-gap structure (EBG)," IEEE Trans. Antennas Propag., vol. 59, no. 5, pp. 1528–1534, 2011.

[10] S. Barth, and A. K. Iyer, "A Miniaturized Uniplanar Metamaterial-Based EBG for Parallel-Plate Mode Suppression," IEEE Trans. Microw. Theory Tech., vol. 64, no. 4, pp. 1176–1185, 2016.

[11] D. Sievenpiper, L. Zhang, R. F. J. Broas, N. G. Alex´opolous, and E. Yablonovitch, "High-impedance electromagnetic surfaces with a forbidden frequency band," IEEE Trans. Microw. Theory Tech., vol. 47, no. 11, pp. 2059–2074, 1999.

[12] J. Y. Deng, J. Y. Li, L. Zhao, L. X. Guo, "A Dual-Band Inverted-F MIMO Antenna With Enhanced Isolation for WLAN Applications ," IEEE Antennas Wireless Propag. Lett., vol. 6, pp. 2270 - 2273, 2017.

[13] S. Rajagopal, G. Chennakesavan, D. R. P. Subburaj, R. Srinivasan, and A. Varadhan, "A dual polarized antenna on a novel broadband multilayer Artificial Magnetic Conductor backed surface for LTE/CDMA/GSM base station applications," AEU- Int. J. Electron. Commun., vol. 80, pp. 73–79, 2017.

[14] H. Lee, B. Lee, "Compact Broadband Dual-Polarized Antenna for Indoor MIMO Wireless Communication Systems," IEEE Trans. Antennas Propag., vol. 64, pp. 766 - 770, 2016.

[15] E. Ameri, S. H. Esmaeli, and S. H. Sedighy, "Wide band radar cross section reduction by thin AMC structure," AEU- Int. J. Electron. Commun., vol. 93, pp. 150–153, 2018.

[16] S. Ghosh, T. N. Tran, T. L. Ngoc, "Dual-Layer EBG Based Miniaturized Multi-Element Antenna for MIMO Systems," IEEE Trans. Antennas Propag., vol. 62, no. 8, pp. 3985 - 3997, 2014.

[17] X. Y. Liu, Y. H. Di, H. Liu, Z. Wu, and M. M. Tentzeris, "A Planar Windmill-like Broadband Antenna Equipped with Artificial Magnetic Conductor for Off-Body Communications," IEEE Antennas Wireless Propag. Lett., vol. 15, pp. 64 - 67, 2015.

[18] S. Yang, Y. Chen, C. Yu, Y. Gong, and F. Tong, "Design of a Low-Profile, Frequency- Reconfigurable, and High Gain Antenna Using a Varactor-Loaded AMC Ground," IEEE Access, vol. 8, pp. 158635- 158646, 2020.

[19] J. Zhu, S. Li, S. Liao; Q. Xue, "Wideband Low-Profile Highly Isolated MIMO Antenna with Artificial Magnetic Conductor," IEEE Antennas Wireless Propag. Lett., vol. 17 pp. 458 - 462, 2018.

[20] A. Ghosh, V. Kumar, G. Sen, S. Das, "Gain enhancement of triple-band patch antenna by using triple-band artificial magnetic conductor," IET Microw. Antennas Propag., vol. 12, no. 8, pp. 1400-1406, 2018.

[21] N. Othman, N. A. Samsuri, M. Ka. A. Rahim, and K. Kamardin, "Low specific absorption rate and gain-enhanced meandered bowtie antenna utilizing flexible dipole-like artificial magnetic conductor for medical application at 2.4 GHz," Microw Optical. Tech Lett., vol. 62, pp. 3881-3889, 2020.

[22] R. C. Hadarig, M. E. de Cos and F. L. Heras, "Novel miniaturized artificial magnetic conductor," IEEE Antennas Wireless Propag. Lett., vol. 12, pp. 174–177, 2013.

[23] A. S. d. Sena, D. B. d. Costa, Z. Ding, P. H. J. Nardelli, "Massive MIMO–NOMA Networks With Multi-Polarized Antennas," IEEE Trans. Wireless Commun.. vol. 18, pp. 5630 - 5642, 2019.

[24] Z. Xu, and C. Deng, "High-Isolated MIMO Antenna Design Based on Pattern Diversity for 5G Mobile Terminals," IEEE Antennas Wireless Propag. Lett., vol. 19 pp. 467 - 471, 2020.

[25] Z. Wang, G. Zhang, Y. Yin, and J. Wu, "Design of a Dual-Band High-Gain Antenna Array for WLAN and WiMAX Base Station," IEEE Antennas Wireless Propag. Lett., vol. 13, pp. 1721 - 1724, 2014.

[26] S. Jam and H. Malekpoor, "Analysis on wideband patch arrays using unequal arms with equivalent circuit model in X-band", IEEE Antennas Wireless. Propag. Lett., vol. 15, pp. 1861-1864, 2016.

[27] H. Malekpoor, and M. Hamidkhani "Bandwidth and gain improvement for reduced size of stacked microstrip antenna fed by folded triangular patch with half V-shaped slot," International Journal of RF and Microwave Computer-Aided Engineering., vol. 31, no. 6, e22649, 2021.

[28] M. Hamidkhani, H. Malekpoor, and Homayoon Oraizi, "Oscillator Phase-Noise Reduction Using High-

Qsc Active Giuseppe Peano Fractal Resonators", IEEE Microw. and Wireless Components Letters., Vol. 29, pp. 354-356, 2019.
[29] J. Joubert, J. C. Vardaxoglou, W. G. Whittow, and J. W. Odendaal, "CPW-fed cavity-backed slot radiator loaded with an AMC reflector," IEEE Trans. Antennas Propag., vol. 60, no. 2, pp. 735–742, 2012.
[30] D. Feng, H. Zhai, L. Xi, S. Yang, K. Zhang, D. Yang, "A Broadband Low-Profile Circular-Polarized Antenna on an AMC Reflector," IEEE Antennas Wireless Propag. Lett., vol. 16, pp. 2840 - 2843, 2017.
[31] H. Malekpoor and S. Jam, "Improved radiation performance of low profile printed slot antenna using wideband planar AMC surface," IEEE Trans. Antennas Propag., vol. 64, no. 11, pp. 4626–4638, 2016.
[32] G. Andrea Casula, F. Lestini, F. Paolo Chietera, G. Muntoni, C. Occhiuzzi, L. Catarinucci, R. Colella, G. Montisci, G. Marrocco, "Design of On-Body Epidermal Antenna on AMC Substrate for UHF RFID in Healthcare," IEEE Trans. Antennas Propag., vol. 72, no. 5, pp. 4023 - 4035, 2024.
[33] Y. W. Zhong, G. M. Yang and L. R. Zhong, "Gain enhancement of bow-tie antenna using fractal wideband artificial magnetic conductor ground," Electron. Lett., vol. 51, no. 4, pp. 315-317, 2015.
[34] J. P. Turpin, Q. Wu, D. H. Werner, B. Martin, M. Bray, and E. Lier, "Near-zero-index metamaterial lens combined with AMC metasurface for high-directivity low-profile antennas", IEEE Trans. Antennas Propag., vol. 62, no. 4, pp. 1928–1936, 2014.
[35] H. R. Raad, A. I. Abbosh, H. M. Al-Rizzo and D. G. Rucker, "Flexible and compact AMC based antenna for telemedicine applications," IEEE Trans. Antennas Propag., vol. 61, no. 2, pp. 524–531, 2013.
[36] Y. Luo, X. Wang, N. Yan, W. An, K, Ma, "Low-Profile Wide Axial-Ratio Beamwidth Circularly Polarized Antenna Loaded With Artificial Magnetic Conductor," IEEE Antennas Wireless Propag. Lett., vol. 23, no. 3, pp. 935 - 939, 2024.
[37] W. Luo, P. Wang, "A Compact UHF-RFID Tag Antenna With Embedded AMC for Metallic Objects", IEEE Antennas Wireless Propag. Lett., vol. 22, no. 4, pp. 873 - 877, 2023.
[38] H. Cheng, G. Xiao, X. Wang, "A Low-Profile Wideband Patch Antenna With Modified Parasitic Mushroom Structures on Nonperiodic AMC," IEEE Antennas Wireless Propag. Lett., vol. 22, no. 4, pp. 719 - 723, 2023.



Hossein Malekpoor was born in Iran, in 1985. He joined the faculty of the Arak University in 2017, where he is currently an Assistant Professor with the Electrical Engineering Department. His research interests include different antennas design, wideband microstrip antennas for UWB applications and wireless communication, analysis of antenna with equivalent circuit models, phased array antennas, designing the periodic structures such as EBGs, AMCs and FSSs, and antenna design with EBG and AMC surfaces.



Mehdi Hamidkhani was born in Esfahan, Iran, in 1985. He received the B.E. degree in electrical engineering from the Yazd University, Iran, in 2007, and the M.Sc. degree in electrical engineering from the Iran University of Science and Technology (IUST), Tehran, Iran, in 2010, and the Ph.D. degree in electrical engineering from the Shiraz University, Shiraz, Iran, in 2016. He is currently a professor assistant at the Islamic Azad University Dolatabad Branch, Isfahan, Iran. His current research interests are RF microwave circuits, Antenna, wireless networks, IoT.